Constrained optimization of fuel efficiency for RCCI engines

Available online at www.sciencedirect.com

ScienceDirect

IFAC Papers Online CONFERENCE PAPER ARCHIVE

IFAC PapersOnLine 52-5 (2019) 648–653

Constrained Optimization of Fuel Efficiency for RCCI Engines ⋆

Lu Xia * **Robbert Willems** * **Bram de Jager** *
Frank Willems *,**

* *Dept. Mechanical Eng., Eindhoven University of Technology (TU/e), Netherlands (e-mail: {l.xia1, r.c.willems, a.g.de.jager, f.p.t.willems}@tue.nl).*
** *TNO Automotive, Helmond, Netherlands.*

Abstract: Fuel efficiency optimization and emission reduction have become essential parts of engine research, due to the growing demand for environmental protection. In this paper, a computationally efficient optimization method has been applied to maximize the fuel efficiency under constraints of maximum pressure rise rate and various pollutant emissions using the combination of multiple regression analysis and particle swarm optimization. This optimization method has been applied to a Reactivity Controlled Compression Ignition (RCCI) engine. First, a data-driven model has been identified, which shows good agreement with experimental data for gIMEP as well as emissions. Using this RCCI model in the proposed optimization method, the optimal operating conditions for highest gross indicated thermal efficiency are determined under various conflicting emission and safety constraints.

Keywords: engine efficiency optimization, particle swarm optimization, multiple regression, reactivity controlled compression ignition.

1. INTRODUCTION

Reactivity Controlled Compression Ignition (RCCI) is a premixed, dual-fuel combustion concept, which has shown to provide very high thermal efficiency and low NOx and soot emissions simultaneously, see, e.g., Reitz and Duraisamy (2015). The most common characteristic for RCCI is to use a low-reactivity fuel, like gasoline, as pre-mixed charge and a high-reactivity fuel, like diesel, as direct injection to promote auto-ignition. The utilization of two fuels with different reactivities provides engines larger control flexibility compared to mono fuel combustion strategies like Homogeneous Charge Compression Ignition (HCCI) and Partially Premixed Combustion (PPC). The RCCI combustion process can be controlled by changing relative amounts of port fuel injection (low-reactivity fuel) and direct injection (high-reactivity fuel), implementing multiple direct injections or varying the direct injection timing.

With growing system complexity, engine control is no longer straight forward. More precisely, due to the growth of the applied air and fuel path actuators and increasingly strict requirements on robust real-world performance, engine calibration time and costs are foreseen to show continuous exponential growth; especially, when map-based control approaches are followed. As a result, model-based approaches are of great interest. However, a systematic, control-oriented optimization method regarding multiple parameters to obtain highest efficiency is still under research, as shown in, e.g., Willems (2018).

Eriksson and Sivertsson (2016) minimized the fuel consumption by searching the optimal combustion trace for a pseudo two-zone model, with constraint of maximum pressure rise rate (MPRR), maximum pressure (MP), knock and NO, using numerical optimal control software CasADi. A similar heat release shaping process is applied for RCCI combustion in Guardiola et al. (2017), where the selection of gasoline fraction is studied under fuel consumption minimization scenario with MPRR and MP limitation. The aforementioned optimizations are generally implemented on physics-based models with indirect or direct correlation to a single operating input.

In Dempsey and Reitz (2011), a computational optimization has been applied to the gasoline-diesel RCCI engine with a low compression ratio using a multi-dimensional CFD model and nondominated sorting genetic algorithm (NSGA II). Six objectives, including NOx, PM, CO, unburned hydrocarbons (HC), indicated specific fuel consumption (ISFC), and MPRR, have been minimized simultaneously by varying six engine design parameters. A similar optimization approach has also been applied to natural gas (NG)-diesel RCCI in Nieman et al. (2012) and methanol-diesel RCCI in Li et al. (2014) using the same computational tools. Bendu et al. (2017) applied multi-objective optimization to an ethanol fuelled HCCI engine by evaluating a fitness function with different priority on each objective using hybrid generalized regression neural network and particle swarm optimization. A similar multi-objective optimization study is applied in Zhang et al. (2017) to experimentally optimize a diesel engine using an improved artificial bee colony algorithm.

In this paper, a computationally efficient optimization method has been applied to a RCCI engine to maximize the gross Indicated Mean Effective Pressure (gIMEP) with respect to a fixed amount of total fuel energy, using multiple linear regression analysis and particle swarm optimization. Compared to the aforementioned multi-objective optimization studies, the proposed method deals with a large number of conflicting constraints by adding penalty functions to the cost function, where the highest gross indicated efficiency can be achieved under various conflicting constrained conditions, such as MPRR, maximum engine-out NOx, PM, CO and HC emissions. Furthermore, the influence of different constraints on the engine performance has also be studied by tuning different weights of penalties.

⋆ This work is supported by the research programme "Towards a HiEff engine" through the Netherlands Organisation for Scientific Research under STW project 14927.

10.1016/j.ifacol.2019.09.103

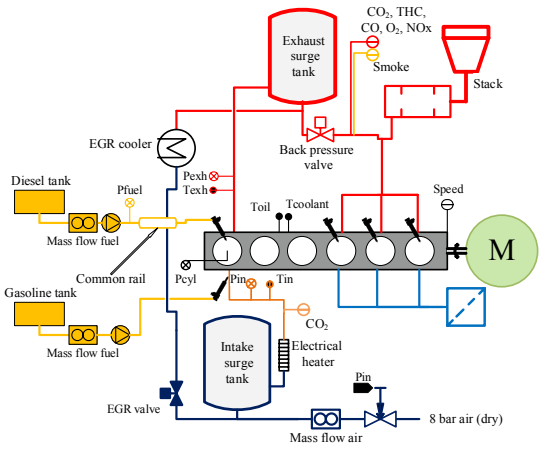

Fig. 1. Schematic of engine test setup based on Willems et al. (2018)

2. EXPERIMENT SETUP

All the datasets employed in this paper are generated on a DAF XEC engine in the TU/e engine lab. A schematic is shown in Fig. 1, where a 2.1 liter single cylinder is isolated as the test cylinder and cylinder 4-6 are operated by stock DAF engine control unit to control crankshaft speed in cylinder 1. The in-cylinder pressure is measured by an AVL GU21C uncooled transducer and a Heidenhain ROD 420 3600 rotary encoder is employed to collect the crank angle information. In addition, gaseous emissions are measured using a Horiba analyser, whereas PM is detemined based on the correlation with Filter Smoke Number (FSN), which is obtained from an AVL 415S smoke meter. A detailed description of the test setup can be found in Willems et al. (2018). The engine specifications and operating conditions are given in Table 1.

To demonstrate the potential of the proposed method, an arbitrary mid-load point with gIMEP at 800 [kPa], has been investigated at a constant engine speed for varying start of actuation for direct injection ($\mathrm{SOA_{DI}}$), exhaust gas recirculation (EGR) rate and ratio of injected port fuel energy to direct injection, namely blend ratio (BR). According to the definition of RCCI from Reitz and Duraisamy (2015), a well-mixed charge of gasoline, air and recirculated gas will be introduced to the combustion chamber at the intake valve opening and a single injection of diesel fuel will be subsequently employed to control the combustion phasing, where diesel fuel is used as the direct injection and gasoline as the port injection. The operating ranges of the input parameters are shown in Table 2 and the experiments are implemented according to the same design of experiment (DoE) approach as in Willems et al. (2018). It should be noted that the EGR rate in Table 2 is based on volumetric values. Although a fixed amount of total fuel energy ($\mathrm{Qm_{TOTAL}}$) is targeted in this study, there still are some deviations due to oscillating injection pressure or measurement disturbances. Therefore, the $\mathrm{Qm_{TOTAL}}$ will be also considered in the modeling process.

Table 1. Specifications of the engine setup and its nominal operating conditions

PFI fuel	Gasoline (EN228)
DI fuel	Diesel (EN590)
Compression ratio	15.8 [-]
DI rail pressure	52000 [kPa]
Intake pressure	168 [kPa]
Intake temperature	35 [°C]
gIMEP	800 [kPa]
Engine speed	125.6 [rad/s]

Table 2. Input sweep range

Input	Range	Unit
$\mathrm{SOA_{DI}}$	-83 to -66	[°CA ATDC]
EGR rate	31 to 48	[%]
BR	2.6 to 8.3	[-]
$\mathrm{Qm_{TOTAL}}$	39	[kJ/s]

3. DATA-DRIVEN MODELING USING MULTIPLE LINEAR REGRESSION ANALYSIS

In this section, the optimization models are presented. The models are generated using multiple linear regression analysis with interactions, providing accurate descriptions of relationship between input variables, $u_{i,t} \in \{\mathrm{SOA_{DI}}, \mathrm{EGR}, \mathrm{BR}, \mathrm{Qm_{TOTAL}}\}$, and outputs y_t, such as gIMEP, MPRR and engine out emissions like gross indicated specific NOx (gISNOx), gISPM, etc., for sample $t \in 1, \ldots, n$, over n experimental observations. The gross indicated emission gISem is calculated by

$$\mathrm{gIS}em = \frac{\dot{m}_{em}}{\mathrm{gPower}}, \tag{1}$$

where gPower is the gross indicated power and $\dot{m}_{em}$ is the mass flow of em, for $em \in \{\mathrm{NOx}, \mathrm{PM}, \mathrm{CO}, \mathrm{HC}\}$.

Multiple linear regression analysis is a powerful approach to model the relationship between a scalar dependent variable and multiple explanatory variables (Jobson, 1991). It is widely applied in practical applications, due to its linear-in-parameter property, where the system performance can be estimated using the linear combinations of various basis functions. The regression basis function for our model is defined as

$$\mathbf{F}(U_t)\mathbf{1}_{k+1\times 1} = 1 + \sum_{i=1}^{p} u_{i,t} + \sum_{i=1}^{p-1}\sum_{j=i}^{p-1} u_{i,t}u_{j,t}, \tag{2}$$

where $U_t = [u_{1,t}, u_{2,t}, \ldots, u_{p,t}]$ and $k = \frac{p^2+p}{2}$, with p explanatory variables, for sample $t \in 1, \ldots, n$. This basis function describes not only the linear and quadratic relation between input variables and output variable, but also the cross-relation between each inputs. Here, the total energy $\mathrm{Qm_{TOTAL}}$, represented by $u_{p,t}$, will not be involved in the cross-terms, since the deviations are very small which can make the model very sensitive to disturbances. Using least square estimation, the related outputs y_t, such as gIMEP, MPRR, gISNOx and gISPM, at samples t, can be estimated as

$$\hat{y}_t = \mathbf{F}(U_t)\hat{\boldsymbol{b}}, \tag{3}$$

where $\hat{\boldsymbol{b}}$ indicates the regression parameters to be estimated. The accuracy of the regression model is normally evaluated by the coefficient of determination R^2. Generally, a larger R^2 indicates higher accuracy, but absolute errors will be also considered in our paper.

Considering the structure of (2), the basis functions might be highly correlated to each other, which might cause multicollinearity in the regression analysis (Allen, 1997), consequently an ill-conditioned problem. This can be addressed by standardizing the regression coefficients. The standardized coefficients can be obtained by applying regression analysis on the unit normal scaled predictors and response, given by

$$u^*_{i,t} = \frac{u_{i,t} - \bar{u}_i}{s_i} \quad \text{and} \quad y^*_t = \frac{\hat{y}_t - \bar{y}}{s_y}, \tag{4a}$$

where $\bar{u}_i$ and $\bar{y}$ are mean values of the predictor i and the response; s_i and s_y are standard deviations of the predictor i and the response, with $i \in 1, \ldots, p$. Then, the regression model after standardization can be presented as

$$\hat{y}^*_t = \mathbf{F}(U^*_t)\hat{\boldsymbol{\gamma}}, \tag{4b}$$

with $U_t^* = [u_{1,t}^*, u_{2,t}^*, \ldots, u_{p,t}^*]$. The simulation results and validation of the model will be discussed in detail later.

4. OPTIMIZATION ALGORITHM

In this section, the aforementioned data-driven models are further employed to formulate the optimization problems, leading to a quadratically constrained quadratic program.

4.1 Problem Formulation

Besides the fuel economy, factors like operational safety, emissions, and noise level are also very crucial for engines. The limit on the MP will avoid mechanical stress limit. MPRR, calculated by the first derivative of the cylinder pressure, is a favorite indication to the level of vibrations during the combustion process in compression ignition engines. Since the experiments are implemented at mid-load operating condition, the MP will not exceed its limit. Considering the constraints on emissions, CO2 will be generally reduced with the increase of efficiency. NOx can be normally reduced by the lean NOx trap and selective catalytic reduction technology. Due to the low combustion temperature in RCCI, CO and unburned HC emissions will increase, so diesel oxidation catalytic converters are required. However, these after-treatment systems will cause extra costs. So our optimization problem will be constructed by adding the constraints to MPRR, gISNOx, gISPM, gISCO, and gISHC.

The indicated efficiency $\eta_{f,i}$ is a very important parameter that can indicate the efficiency of an engine in converting fuel energy to work during each cycle (Eriksson and Nielsen, 2014). For a dual fuel engine, $\eta_{f,i}$ is specified by

$$\eta_{f,i} = \frac{W_{\mathrm{i}}}{\mathrm{Qm}_{\mathrm{TOTAL}}}, \tag{5}$$

with $\mathrm{Qm}_{\mathrm{TOTAL}} = m_{\mathrm{PFI}} q_{\mathrm{LHV}_{\mathrm{pfi}}} + m_{\mathrm{DI}} q_{\mathrm{LHV}_{\mathrm{di}}}$, where m_{PFI} and m_{DI} are the mass of gasoline and diesel fuel injected to the engine for each cycle, $q_{\mathrm{LHV}_{\mathrm{pfi}}} = 44$ [kJ/g] and $q_{\mathrm{LHV}_{\mathrm{di}}} = 43$ [kJ/g] are the approximated specific heating values and W_{i} is the indicated work generated by the engine. Another essential parameter is the IMEP, which is proportional to W_{i} in each cycle, given by

$$\mathrm{IMEP} = \frac{W_{\mathrm{i}}}{V_{\mathrm{d}}}. \tag{6}$$

where V_{d} is the displaced volume. Based on the definition above, the highest indicated efficiency can be achieved by maximizing the IMEP with respect to the total energy converted from the fixed amount of fuel injected ($\mathrm{Qm}_{\mathrm{TOTAL}}$), realizing an energy-based optimization problem. Due to the fixed valve events and displacement volume in our test setup, our optimization objective will be focused on gross IMEP (gIMEP), given by

$$\begin{aligned} \max_{U_t \in \mathbb{R}^p} \quad & \mathrm{gIMEP}(U_t) && \text{(7a)}\\ \text{s.t.} \quad & \mathrm{Qm}_{\mathrm{TOTAL}} = \text{constant} && \text{(7b)}\\ & U_{min} \le U_t \le U_{max} && \text{(7c)}\\ & \mathbf{G}(U_t) \le \mathbf{C} && \text{(7d)} \end{aligned}$$

with

$$\mathbf{C} = \begin{bmatrix} \mathrm{MPRR}_{max} \\ \mathrm{gISNOx}_{max} \\ \mathrm{gISPM}_{max} \\ \mathrm{gISCO}_{max} \\ \mathrm{gISHC}_{max} \end{bmatrix}, \tag{7e}$$

and $\mathbf{G}(U_t)$ is a vector function, indicating different constraints, where U_{min} and U_{max} are the boundaries of the input variables, guaranteeing the feasibility of the data-driven models. By checking the Hessian matrix of the objective function and constraints, it turns out that (7) is a non-convex optimization problem, indicating the existence of local optima.

4.2 Particle Swarm Optimization

Particle swarm optimization (PSO) is a very popular method for solving unconstrained global optimization problems (Marini and Walczak, 2015). It is inspired by the artificial life like bird flocking and is widely applied in many applications, owing to its large flexibility in dealing with optimization problems with nonlinearities. The optimal solution is found by searching the best position among a group (swarm) of candidate (particle) solutions by comparing particle's own best performance to their neighbors' best performance.

In the PSO algorithm, a group of N particles in p-dimensional space is defined as:

$$\mathbf{U} = \{U_1, U_2, \ldots, U_N\}, \tag{8a}$$

where

$$U_r = [u_{1,r}, u_{2,r}, \ldots, u_{p,r}] \tag{8b}$$

is the r-th individual particle comprised of p parameters, for $r \in 1, 2, \ldots, N$. By evaluating the cost functions (3) for different particles, the best personal and global positions, represented as P_r and Gp respectively, can be searched based on the following iteration process

$$U_r(\delta + 1) = U_r(\delta) + v_r(\delta + 1), \tag{9a}$$

and the "velocity" of the r-th particle is defined as

$$\begin{aligned} & v_r(\delta + 1) = \\ & c_0 v_r(\delta) + c_1(P_r - U_r(\delta))d_{1,r} + c_2(Gp - U_r(\delta))d_{2,r}, \end{aligned} \tag{9b}$$

where $\delta \in \mathbb{N}$ is the iteration step and c_0 is the inertia weight; c_1 and c_2 are the positive acceleration constants; $d_{1,r}$ and $d_{2,r}$ are random numbers uniformly distributed in $[0, 1]$. The selections of these parameters will influence the convergence of PSO and detailed discussion can be found in Marini and Walczak (2015).

By applying PSO, the maximum gIMEP can be found by searching the optimal combinations of the input variables $\mathrm{SOA}_{\mathrm{DI}}$, EGR and BR for a specific amount of fuel energy. Further, the constraints can be evaluated by adding a penalty function to the cost function (Smith and Coit, 1997), given by

$$\begin{aligned} \max_{U_r \in \mathbb{R}^p} \quad & \mathrm{gIMEP}(U_r) - \sum_{i}^{I} \phi_i(k_i, \mathbf{g}_i) && \text{(10a)}\\ \text{s.t.} \quad & \mathrm{Qm}_{\mathrm{TOTAL}} = \text{constant} && \text{(10b)}\\ & U_{min} \le U_r \le U_{max} && \text{(10c)}\\ & \mathbf{g}(U_r) = \mathbf{G}(U_r) - \mathbf{C} && \text{(10d)} \end{aligned}$$

with

$$\phi_i(k_i, \mathbf{g}_i) = \begin{cases} 0 & \text{for} \quad \mathbf{g}_i \le 0, \\ k_i \mathbf{g}_i^m & \text{for} \quad \mathbf{g}_i > 0, \end{cases} \tag{10e}$$

where $\mathbf{g}(U_r) = [\mathbf{g}_1(U_r), \ldots, \mathbf{g}_i(U_r), \ldots, \mathbf{g}_I(U_r)]^T$ is a vector function, indicating the distance between constraint functions and their upper bounds, and I is the total number of constraints. Considering different units in the objective function and constraints, feature scaling is further applied to normalize the objective function and constraints from 0 to 1, given by

$$\widetilde{\mathrm{gIMEP}}(U_r) = \frac{\mathrm{gIMEP}(U_r) - \mathrm{gIMEP}_{min}}{\mathrm{gIMEP}_{max} - \mathrm{gIMEP}_{min}}$$

and

$$\tilde{\mathbf{g}}_i = \frac{\mathbf{g}_i - \mathbf{g}_{i,min}}{\mathbf{g}_{i,max} - \mathbf{g}_{i,min}};$$

Algorithm 1: Constrained PSO algorithm

for N particles and run=1: Q, $r \in 1:N$
  Initialization
  - Position: $U_r(0) \in [U_{min},\ U_{max}]$
  - Speed: $v_r(0) = 0.01U_r(0)$
  - Personal best position: $p_r(0) = U_r(0)$
  - Global best position: $[Gv(0), Gp(0)] = \max(\mathbf{F}(\mathbf{U}(0))\hat{\boldsymbol{b}})$

  while $Gv(\delta+1) - Gv(\delta) > tol$
    Update particle speed according to (9b)
    Update particle position according to (9a)
    Evaluate constraints according to (10d)
    Evaluate fitness function according to (10a)
    if $\left(\text{gIMEP-}\sum_i^I \phi_i\right)(U_r(\delta+1)) > \left(\text{gIMEP}-\sum_i^I \phi_i\right)(p_r)$
      update personal best position: $p_r = U_r(\delta+1)$
    end if
    if maximum value f_{max} of (10a) over N particles $> Gv(\delta)$
      update global best position:
      $[Gv(\delta+1),\ Gp(\delta+1)] = [f_{max},\ \arg\max(10a)]$
    end if
  end while
  G(run)=$Gp(\delta+1)$
end for
Find maximum value of G

gIMEP_{max} and $\mathbf{g}_{i,max}$ indicate the maximum optimal results within the feasible range, and minimum results for gIMEP_{min} and $\mathbf{g}_{i,min}$; k_i and m are constants, indicating the different penalty on the i-th boundary. Here, we choose $m = 2$ to achieve a strictly increasing continuous function (Smith and Coit, 1997) and k_i will be chosen accordingly based on the importance of each constraint, to deal with multiple conflicting constraints, which will be further discussed in Section 5.2. To guarantee the global convergence of PSO, the iteration has been repeated Q times, where the global optima can be obtained by comparison of Q optimal results. The iteration process of the aforementioned optimization problem is generally presented in Algorithm 1, the unconstrained PSO iteration process can be found in Marini and Walczak (2015).

5. SIMULATION STUDY

In this section, first, the accuracy of the proposed data-driven models will be studied and validated experimentally. The optimization results will be presented under various constrained and unconstrained conditions. It should be noted that all simulation results presented in the following are specific for the engine cell and operating conditions described in Section 2. The optimization approach and the analysis techniques are general and can be repeated for different engine setups with different operating conditions.

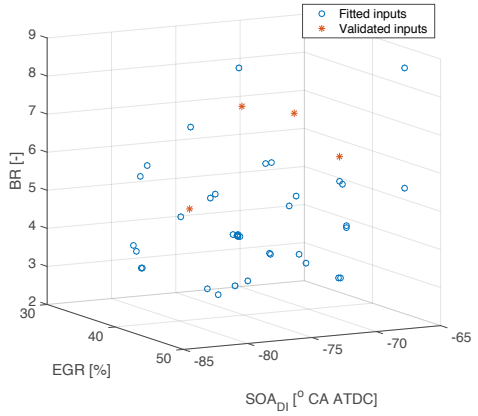

Fig. 2. Randomly distributed input variables for data-driven models validation

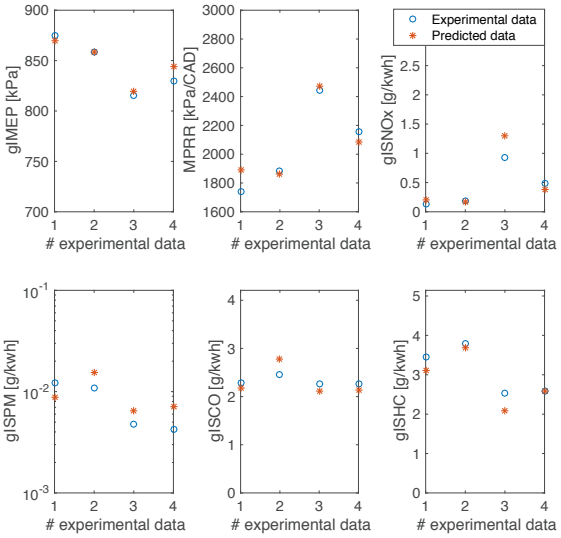

Fig. 3. Validation of predicated outputs.

5.1 Data-driven modeling

The accuracy of the data-driven models are evaluated based on R^2 over 37 sets of experimental data and maximum absolute errors $|e|_{\max}$ between experimental data with gIMEP larger than 820 [kPa] and their fitted responses, since global optima are achieved by maximization of gIMEP, those data with low gIMEP are not valuable for evaluation. A detailed description of accuracy for each response is given in Table 3.

To validate the aforementioned data-driven models, 4 operating points have been implemented on the engine setup with random combination of SOA_{DI}, EGR and BR within the input ranges, shown in Fig. 2. A comparison of the outputs, gIMEP, MPRR, gISNOx, gISPM, gISCO and gISHC, between predicted results and experimental results are given in Fig. 3, where the root-mean-square errors are 7.450 [kPa], 83.090 [kPa/CAD], 0.140 [g/kWh], 0.003 [g/kWh], 0.211 [g/kWh] and 0.231 [g/kWh], respectively, showing accurate predictions of the regression models. These regression models will be employed to formulate the optimization problem and the results will be discussed in the next subsection.

5.2 Optimization results

Due to the data generating method of DoE, the feasible range of the regression models are in a diamond shape. To guarantee the feasibility of the optimization problem, the input constraints in (10) are set as in Table 4, to strictly fit in the model domain.

Table 3. Accuracy of model fit

	R^2	$\lvert e\rvert_{\max}$
gIMEP	0.93	16.52 [kPa]
MPRR	0.94	95.27 [kPa/CAD]
gISNOx	0.95	0.17 [g/kWh]
gISPM	0.93	0.01 [g/kWh]
gISCO	0.94	0.34 [g/kWh]
gISHC	0.92	0.13 [g/kWh]

Table 4. Input constraints

Input	Range	Unit
SOA_{DI}	-80 to -70	[°CA ATDC]
EGR	35 to 47	[%]
BR	3 to 7.6	[-]

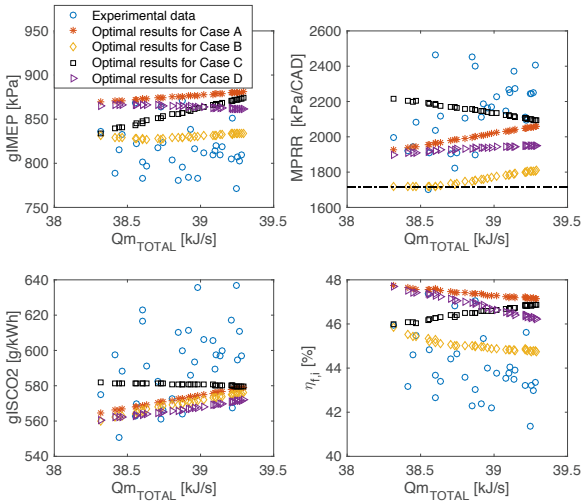

Fig. 4. Comparison of optimal gIMEP, MPRR, gISCO2 and gross indicated efficiency $\eta_{f,i}$ between various constrained and unconstrained conditions, with respect to different amount of fuel energy.

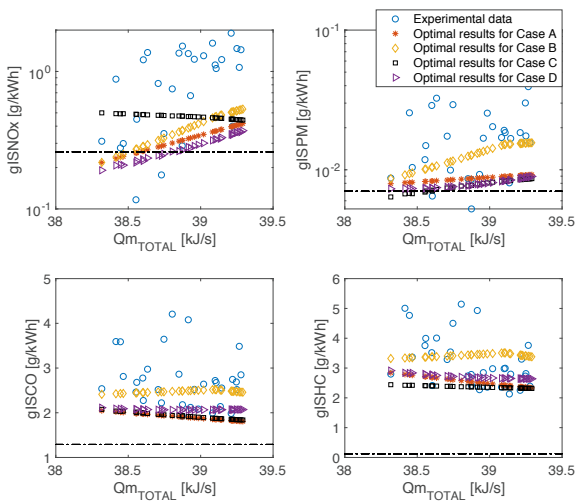

Fig. 5. Comparison of gISNOx, gISPM, gISCO and gISHC between various constrained and unconstrained conditions, with respect to different amount of fuel energy.

Based on the EURO VI emissions constraints, the constraints of gISNOx, gISPM, gISCO and gISHC are set at 0.40 [g/kWh], 0.01 [g/kWh], 1.50 [g/kWh] and 0.13 [g/kWh], respectively, while the constraint of MPRR is arbitrarily set at 1800 [kPa/CAD]. Considering the uncertainties of the regression models in Section 5.1, the model of gISHC is not accurate enough to fit the constraint, but is still required to be minimized. To achieve a robust optimal result, the constraints of gISNOx, gISPM, gISCO and MPRR are deducted by the model uncertainties, set at 0.260 [g/kWh], 0.007 [g/kWh], 1.289 [g/kWh] and 1717 [kPa/CAD], respectively. To study the influence of different constraints on the engine performance, the following conditions will be compared and discussed in this section:

- Case A: unconstrained condition;
- Case B: constrained MPRR;
- Case C: constrained NOx, PM, CO and HC;
- Case D: constrained MPRR, NOx, PM, CO and HC

Considering the aforementioned cases, the penalty in (10e) can be chosen as k_i=0 or $k_i = K$, depending on the availability of each constraint, where K is a constant. For Case A, k_i is chosen to be 0, for $i \in \{1, \ldots, 5\}$, to deactivate the constraints. The minimal values of MPRR, gISNOx, gISPM, gISCO and gISHC, that can be achieved within the feasible range, are 1675 [kPa/CAD], 0.124 [g/kWh], 0.004 [g/kWh], 1.827 [g/kWh] and 1.632 [g/kWh]. Specifically, the gISCO and gISHC will never fit the constraints. Therefore, soft constraints are required to strike a balance among those conflicting constraints, and any penalty can be chosen as long as it is large enough to lead the PSO to choose the largest cost function (10a). Here, we choose $k = [100, 0, 0, 0, 0]$ for Case B. Considering Case C, soft constraints have been applied to emissions, with equal importance, specifically $k = [0, 100, 100, 100, 100]$. Similarly, $k = [100, 100, 100, 100, 100]$ for Case D.

Figure 4 shows the comparison of the optimal gIMEP, MPRR, gISCO2 and $\eta_{f,i}$ between unconstrained and constrained conditions with respect to slightly different amounts of energy consumption, where the black dash-line indicates the level of constraint and the experimental data are indicated by blue circles, showing the corresponding outputs regarding to different input sweeps. Fig. 5 illustrates the comparison of corresponding emissions, such as gISNOx, gISPM, gISCO and gISHC. Comparing these two figures, it can be seen that the maximum gIMEP for the unconstrained optimization (Case A), indicated by red stars, is achieved with lowest gISCO simultaneously, but the corresponding gISCO2 does not necessarily reach the lowest level. The highest $\eta_{f,i}$ is 47.8[%] for the unconstrained condition. For the optimization results with constrained MPRR (Case B), given in yellow diamonds, the gISPM, the gISCO and the gISHC will increase notably, while the gISCO2 will slightly decrease. By limiting the MPRR to 1717 [kPa/CAD], the gIMEP is largely reduced and the highest $\eta_{f,i}$ is 45.8 [%]. It should be noted that the MPRR does not always satisfy the constraint, indicating a MPRR limitation in this operating range.

Further, if we only add constraints to emissions (Case C), such as PM, NOx, CO and HC, indicated by black squares in Fig. 5, the gISPM, the gISCO and the gISHC will reach the lowest levels in this operating range and the gISNOx will be round 0.5 [g/kWh]. However, the gISCO2 and MPRR will increase notably. In this condition, the highest $\eta_{f,i}$ will decrease from 47.8 [%] to 46.9 [%] compared to the unconstrained condition. By adding constraints to MPRR, NOx, PM, CO and HC simultaneously (Case D), given in purple triangles in Figs. 4 and 5, the gISCO2 will reach the lowest level among these four different conditions. Both gISNOx and gISPM will partially satisfy their constraints, but the gISCO and gISHC will increase as the decrease of MPRR, indicating conflicting constraints of these parameters. The maximal achievable $\eta_{f,i}$ will fall from 47.8[%] to 47.7 [%] compared to the unconstrained condition and the highest value of MPRR will decrease from 2060 [kPa] to 1951 [kPa], at sacrifice of gISCO and gISHC. A summary of the optimal outputs, such as highest $\eta_{f,i}$, MPRR, gISNOx, gISPM, gISCO, gISHC and gISCO2, for the aforementioned conditions can be found in Table 5. It can be seen that the lowest CO2 does not necessarily indicate the highest efficiency, but can be accompanied by high CO and HC emissions.

The corresponding optimal inputs for the aforementioned conditions are illustrated in Fig. 6. It can be seen that late SOA_{DI} and high EGR are both required to achieve the highest efficiency for unconstrained and constrained condition, while the EGR will be slightly adjusted according to BR when high proportion of gasoline is employed. The utilization of high proportion of gasoline will reduce PM, CO and HC emissions simultaneously, and will raise MPRR and gIMEP. It is not surprising to see

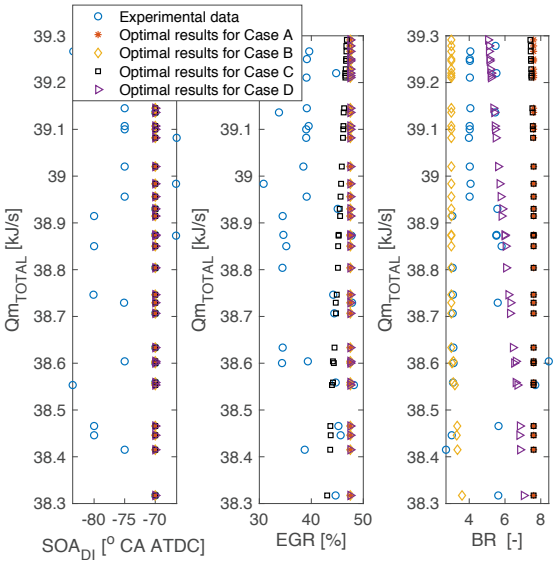

Fig. 6. Comparison of corresponding optimal inputs between various constrained and unconstrained conditions, with respect to different amount of fuel energy.

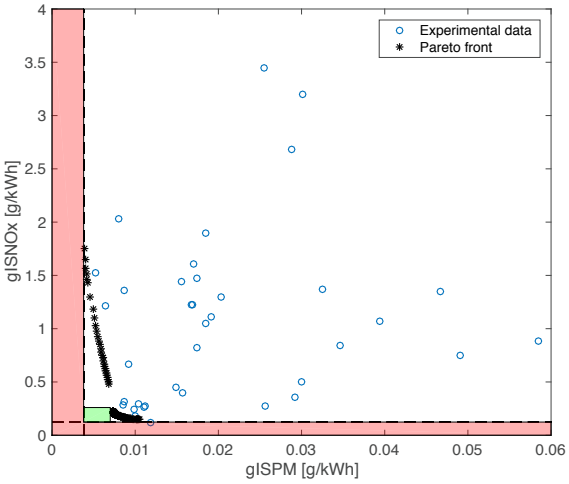

Fig. 7. Pareto front of gISNOx and gISPM for $\mathrm{Qm}_{\mathrm{TOTAL}} = 38.32$ [kJ/s]

that gISNOx is hardly affected by BR, since $\mathrm{SOA}_{\mathrm{DI}}$ is relatively early, where local air-fuel ratios are still lean enough for BR not to make a significant difference in NOx formation. As such, the optimal operating points can be different regarding to different constraints. The highest $\eta_{f,i}$ in this operating range is achieved at $\mathrm{SOA}_{\mathrm{DI}} = -70$ [°CA ATDC], EGR=47.5 [%] and BR=7.6 [-]. Using the proposed method, the optimal solution can be obtained efficiently under various constrained conditions.

Figure 7 shows the Pareto front of gISNOx and gISPM for $\mathrm{Qm}_{\mathrm{TOTAL}} = 38.32$ [kJ/s], where the blue circles indicate the experimental data and Pareto front is given in black stars. The infeasible range is obtained by minimizing gISNOx and gISPM within the input constraints, given in red shadow. The green area indicates operating conditions satisfying the constraints of gISNOx and gISPM. It can be observed that, with the proposed optimization method, the optimal results are always on the Pareto front. A trade off between each constraint can be obtained by setting different values of penalties on each constraint.

Table 5. Summary of optimal outputs for the unconstrained and constrained conditions

Case	A	B	C	D
maximal $\eta_{f,i}$ [%]	47.8	45.8	46.9	47.7
MPRR [kPa/CAD]	1925	1721	2092	1895
gISPM [g/kWh]	0.008	0.011	0.009	0.007
gISNOx [g/kWh]	0.2	0.2	0.4	0.2
gISCO [g/kWh]	2.1	2.7	1.8	2.1
gISHC [g/kWh]	2.8	3.8	2.3	2.9
gISCO2 [g/kWh]	565	560	580	561

6. CONCLUSION

In this paper, a computationally efficient optimization method has been applied to maximize gIMEP for a fixed amount of total energy supply. With the proposed optimization method, the optimal operating points are successfully obtained under various, conflicting constrained conditions like MPRR and emissions, such as NOx, PM, CO and HC. In the simulation study, the accuracy of the proposed data-driven models is validated experimentally, showing accurate predictions of the corresponding outputs, where the largest relative error of gIMEP between predicted results and experimental data is 1.5 [%]. For the studied operating conditions, the engine-out gISCO and gISHC will not satisfy the EURO VI emission limits, so after treatment systems are required. Within the EURO VI constraints for engine-out gISNOx and gISPM, the highest indicated efficiency that can be achieved is 47.7 [%]. As offline optimization is limited to the range of DoE, further work will be focused on combining PSO with DoE for different sweeps of $\mathrm{Qm}_{\mathrm{TOTAL}}$, in order to iteratively search for the global optima online.

REFERENCES

Allen, M.P. (1997). *The problem of multicollinearity*, 176–180. Springer US, Boston, MA.

Bendu, H., Deepak, B., and Murugan, S. (2017). Multi-objective optimization of ethanol fuelled HCCI engine performance using hybrid GRNN–PSO. *Applied Energy*, 187, 601–611.

Dempsey, A.B. and Reitz, R.D. (2011). Computational optimization of reactivity controlled compression ignition in a heavy-duty engine with ultra low compression ratio. *SAE Int. J. Engines*, 4(2), 2222–2239.

Eriksson, L. and Nielsen, L. (2014). *Modeling and Control of Engines and Drivelines*. John Wiley & Sons.

Eriksson, L. and Sivertsson, M. (2016). Calculation of optimal heat release rates under constrained conditions. *SAE Int. J. Engines*, 9(2), 1143–1162.

Guardiola, C., Pla, B., Garcia, A., and Boronat, V. (2017). Optimal heat release shaping in a reactivity controlled compression ignition (RCCI) engine. *Control Theory Technology*, 15, 117–128.

Jobson, J. (1991). *Applied Multivariate Data Analysis Volume I: Regression and Experimental Design*. Springer-Verlag New York.

Li, Y., Jia, M., Chang, Y., Liu, Y., Xie, M., Wang, T., and Zhou, L. (2014). Parametric study and optimization of a RCCI (reactivity controlled compression ignition) engine fueled with methanol and diesel. *Energy*, 65, 319–332.

Marini, F. and Walczak, B. (2015). Particle swarm optimization (PSO). A tutorial. *Chemometrics and Intelligent Laboratory Systems*, 149, 153–165.

Nieman, D.E., Dempsey, A.B., and Reitz, R.D. (2012). Heavy-duty RCCI operation using natural gas and diesel. *SAE Int. J. Engines*, 5(2), 270–285.

Reitz, R.D. and Duraisamy, G. (2015). Review of high efficiency and clean reactivity controlled compression ignition (RCCI) combustion in internal combustion engines. *Progress in Energy and Combustion Science*, 46, 12–71.

Smith, A.E. and Coit, D.W. (1997). Penalty functions. *Handbook of evolutionary computation*, 97(1), C5.2.

Willems, F. (2018). Is cylinder pressure-based control required to meet future HD legislation? *IFAC-PapersOnLine*, 51(31), 111–118.

Willems, R., Bakker, P., Dreezen, R., and Somers, B. (2018). The impact of operating conditions on post-injection efficacy; a study using Design-of-Experiments (no. 2018-01-0229). In *WCX World Congress Experience*. SAE International.

Zhang, Q., Ogren, R.M., and Kong, S.C. (2017). Application of improved artificial bee colony algorithm to the parameter optimization of a diesel engine with pilot fuel injections. *Journal of Engineering for Gas Turbines and Power*, 139(11), 112801.